Supplement of Clim. Past, 17, 2327–2341, 2021
https://doi.org/10.5194/cp-17-2327-2021-supplement

Climate of the Past
Open Access

Supplement of

Freshwater routing in eddy-permitting simulations of the last deglacial: the impact of realistic freshwater discharge

Ryan Love et al.

Correspondence to: Ryan Love (rlove@mun.ca)

S1 Supplemental Figures

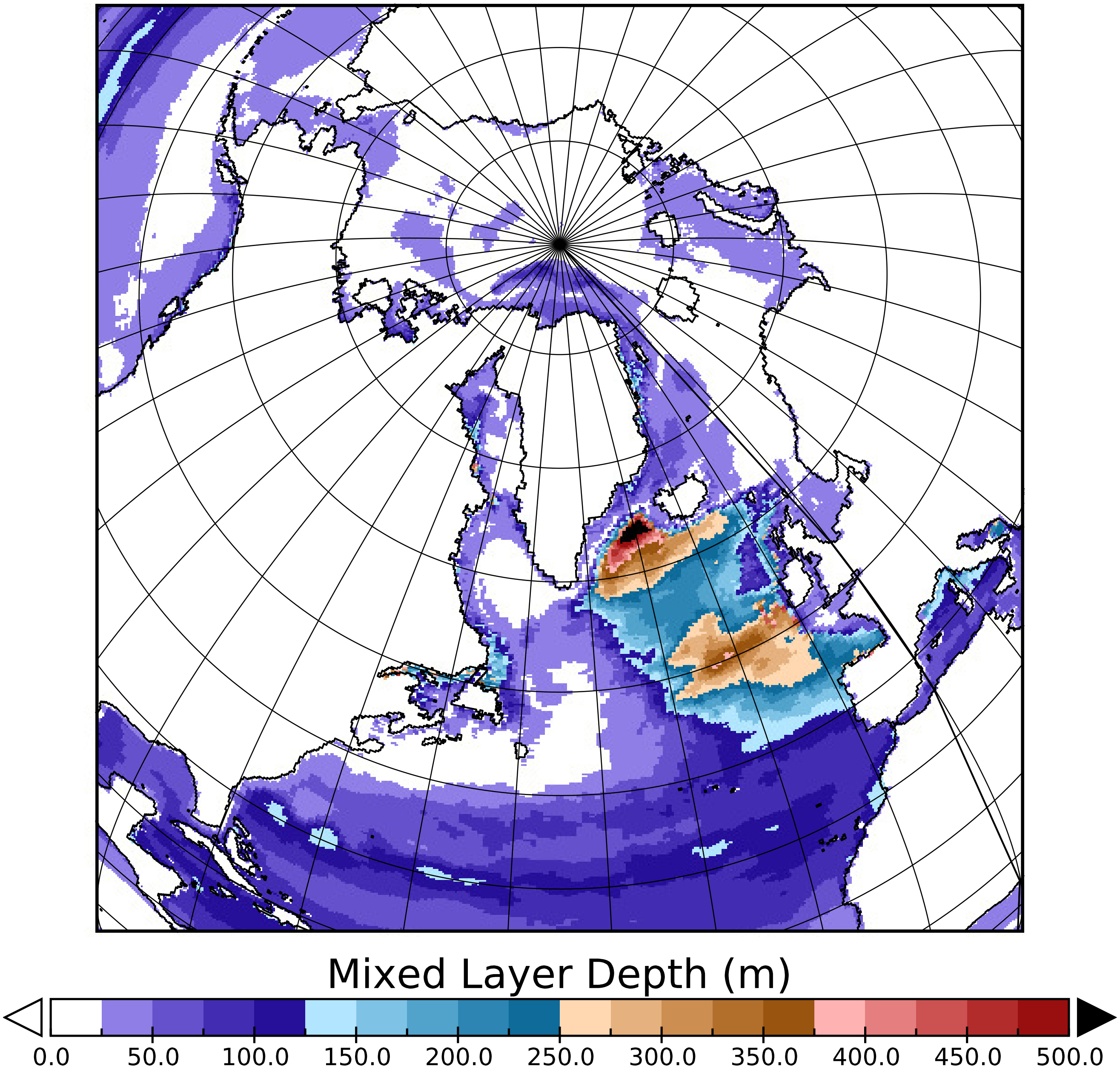

Figure S1: Mixed layer depth in the North Atlantic from the last 5 years of our open Bering Strait control simulation. The most significant region of mixing is between -40E to 0E, 50N to 65N. This is the region which we examine the salinity anomaly to evaluate the impact of each of our injection scenarios. Latitude and longitude lines represent 10 degree increments.

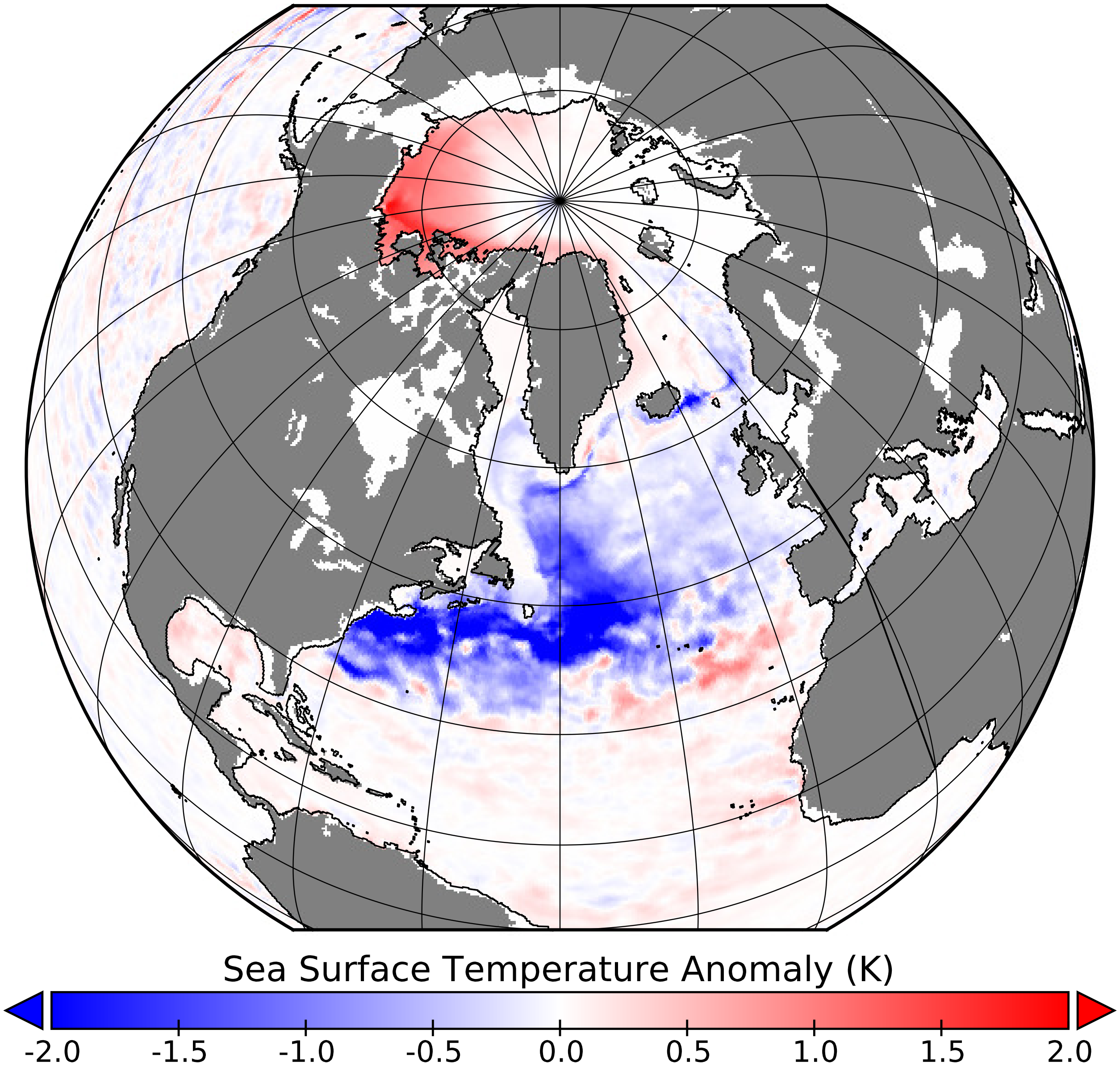

Figure S2: Sea surface temperature differences for the closed Bering Strait 2dSv Mackenzie River forcing. Given our model configuration is uncoupled the differences observed here should be used only for context.

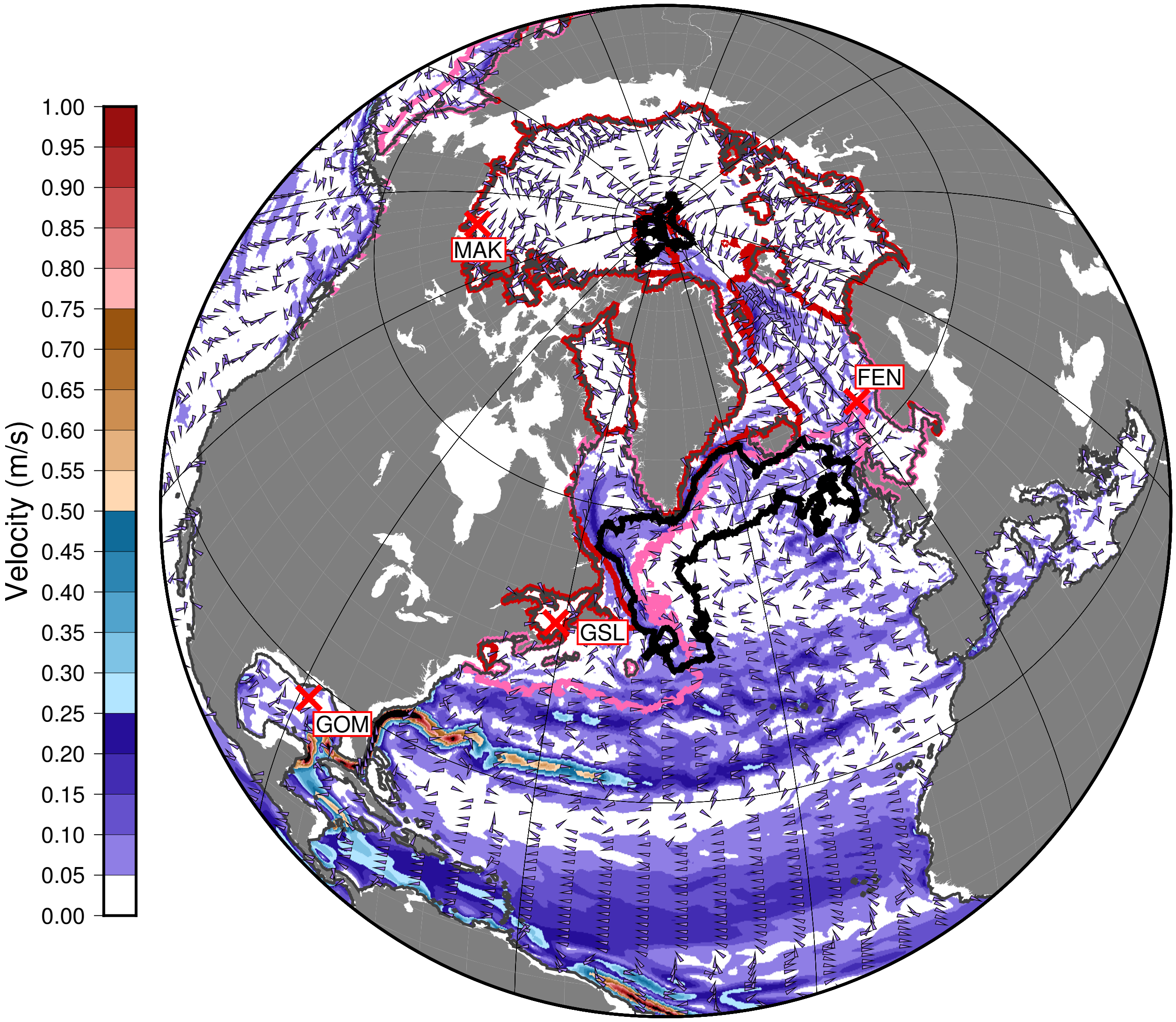

Figure S3: Average sea surface velocity for the last 5 years of our CBS Control run with arrows denoting the direction. Present day land-sea mask is shown in light grey while simulation land-sea mask is contoured in a darker shade of grey. The dark red and pink contours denotes the time minimum and maximum sea ice extent respectively, of at least 15% sea ice coverage calculated over the last 5 years of the simulation. When comparing the sea ice maximal extent to the mixed layer depth shown in S1 (for the OBS case) and black contour, denoting 1000m mixed layer depth, in the current plot we see the mixing is just off the outer limit of the sea ice maximum. The arrows denoting direction are shown at a lesser density than the native grid to aid in visualization.

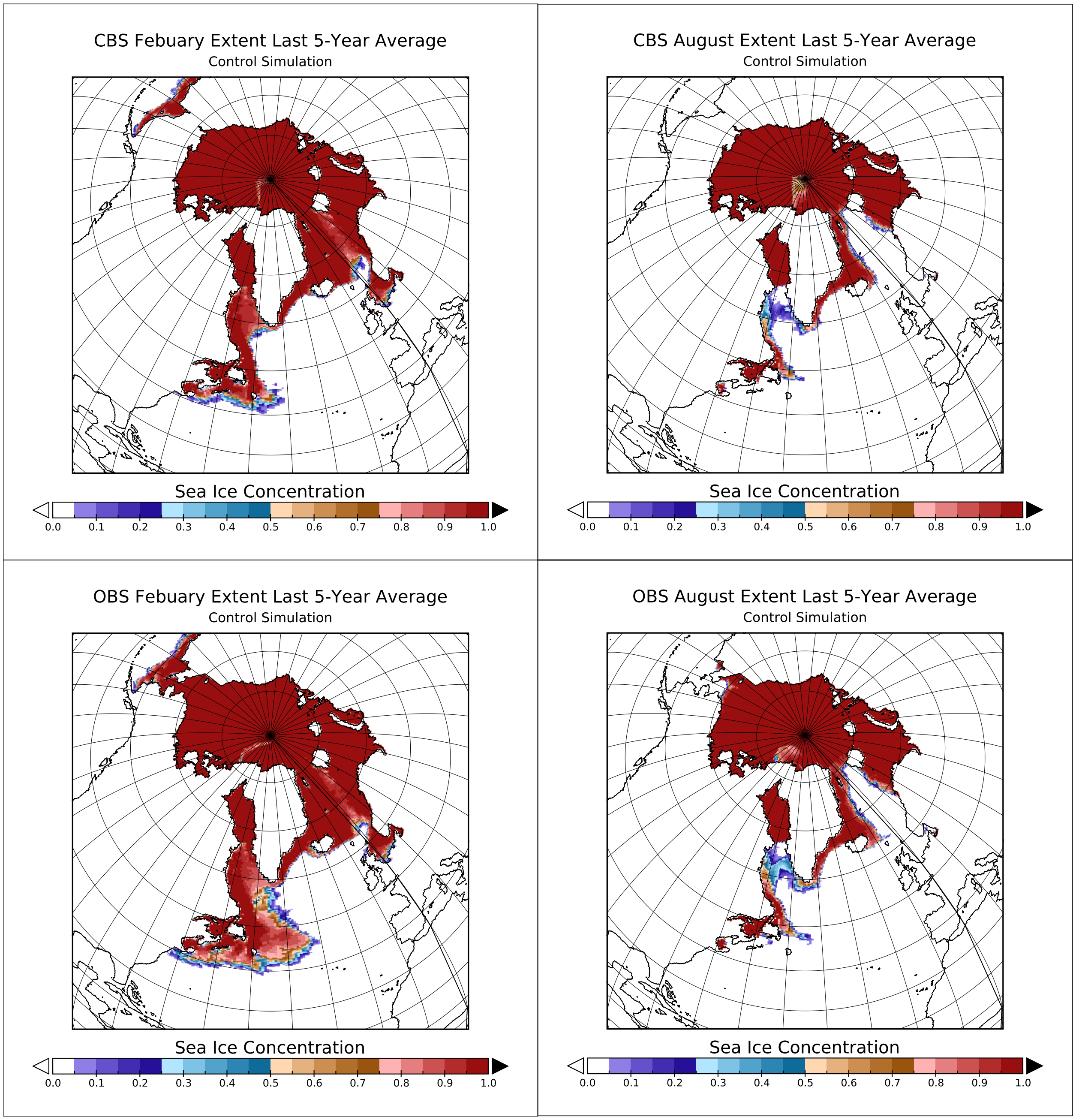

Figure S4: Sea ice minimal and maximal extent for both the open and closed Bering Strait control simulations. Sea ice concentration values range from 0 (no sea ice) to 1 (full grid cell coverage). Minimum/maximum extents correspond to August and February respectively, the averages are generated as monthly means from the last 5 years of simulation data for each run (whose duration is approximately 30 simulation years each).

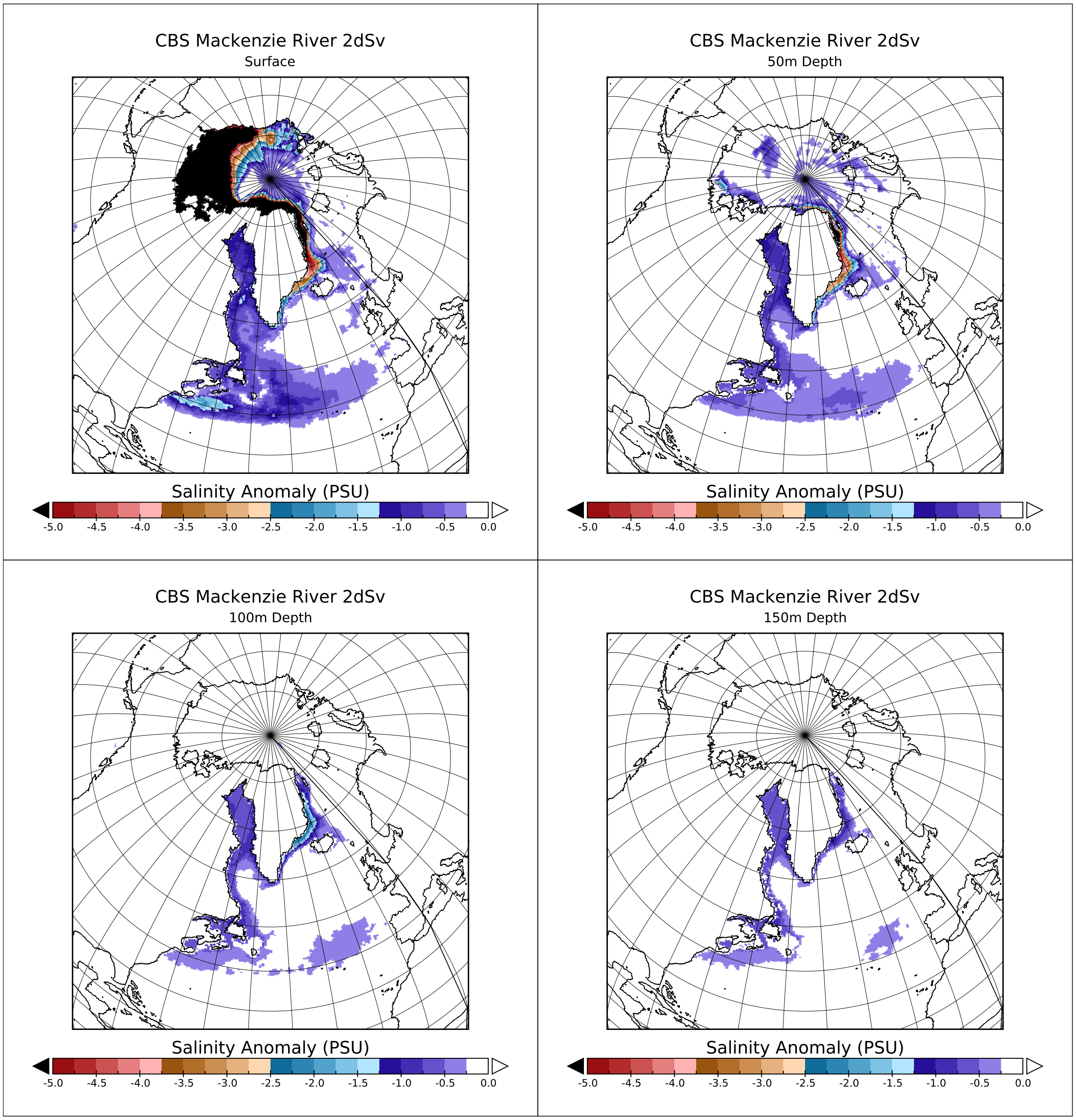

Figure S5: Salinity anomaly distribution at a selection of depths for the Closed Bering Strait Mackenzie River 2dSv continual injection scenario. This distribution is the average of the anomaly field over the last 5 years of model integration.

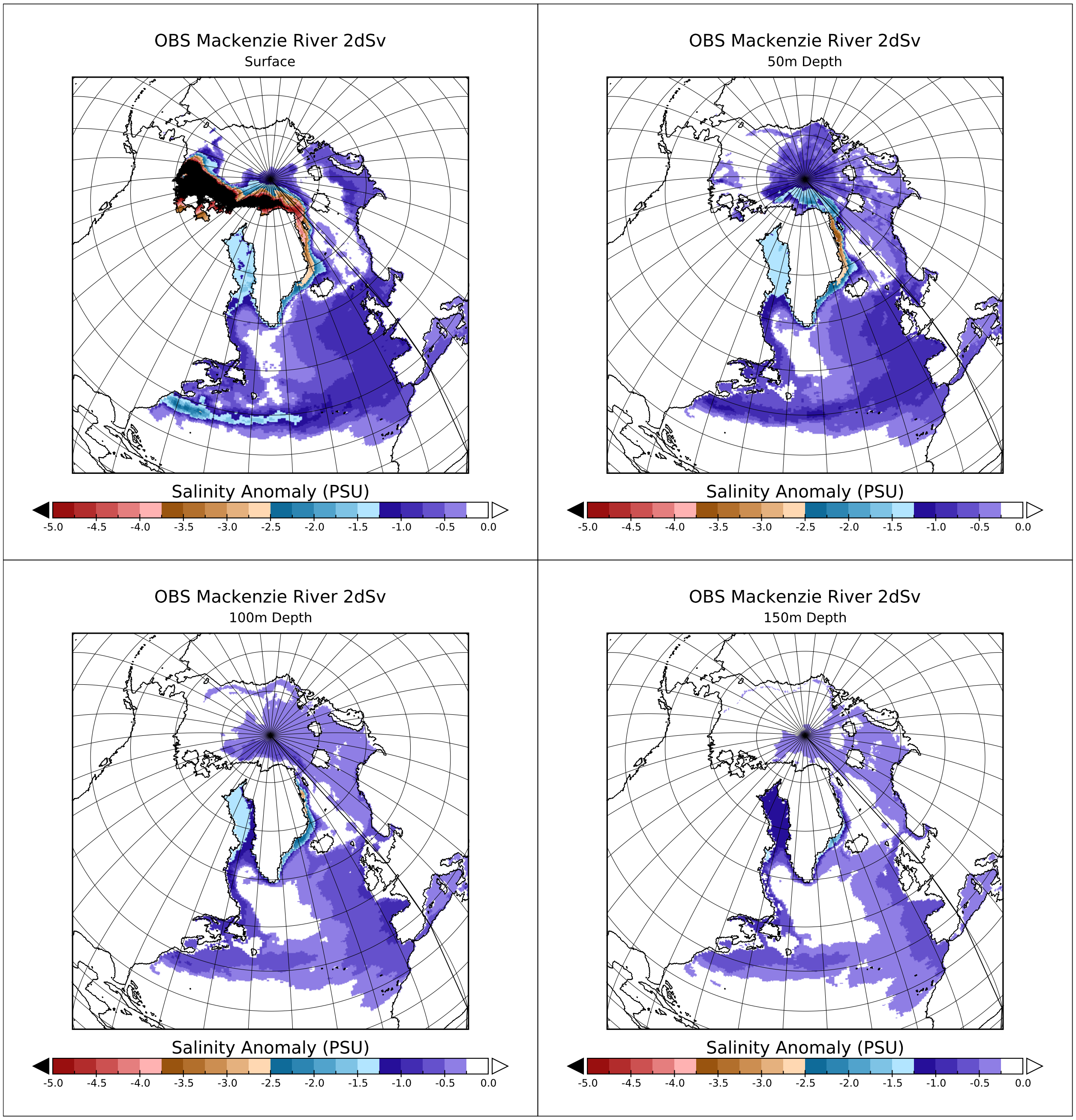

Figure S6: Salinity anomaly distribution at a selection of depths for the Open Bering Strait Mackenzie River 2dSv continual injection scenario. This distribution is the average of the anomaly field over the last 5 years of model integration.

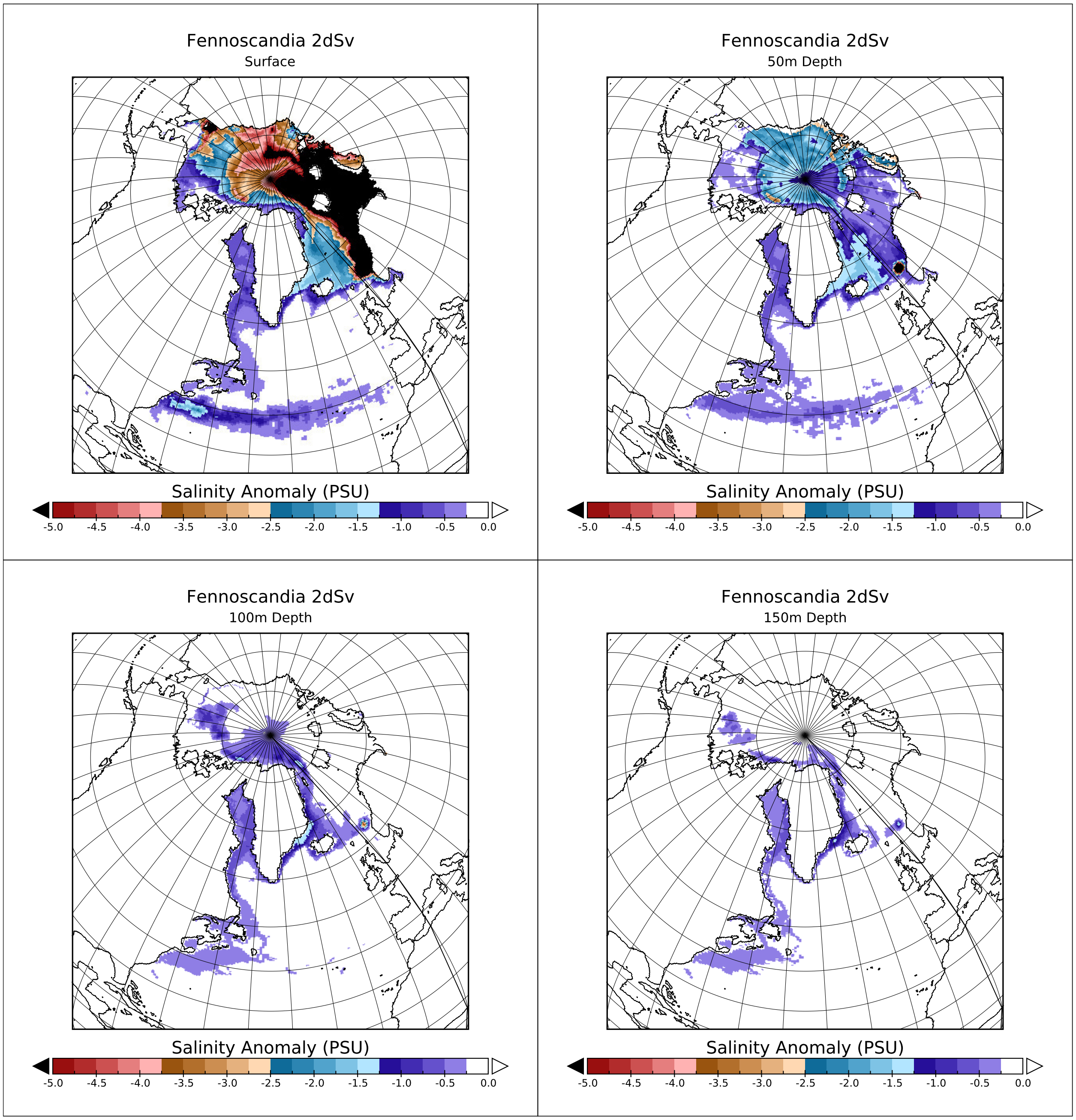

Figure S7: Salinity anomaly distribution at a selection of depths for the Open Bering Strait Fennoscandia 2dSv continual injection scenario. This distribution is the average of the anomaly field over the last 5 years of model integration.

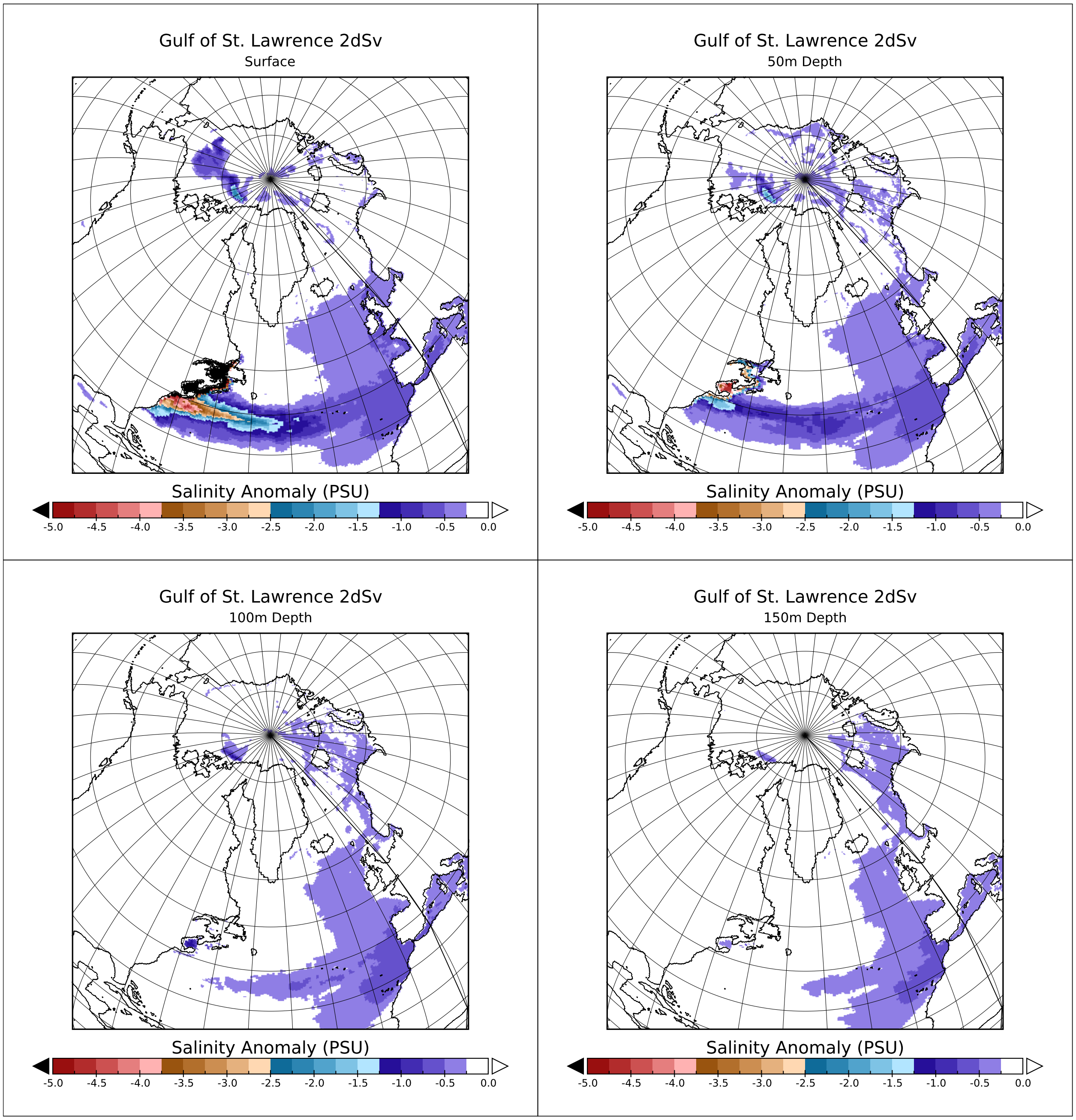

Figure S8: Salinity anomaly distribution at a selection of depths for the Open Bering Strait Gulf of St. Lawrence 2dSv continual injection scenario. This distribution is the average of the anomaly field over the last 5 years of model integration.

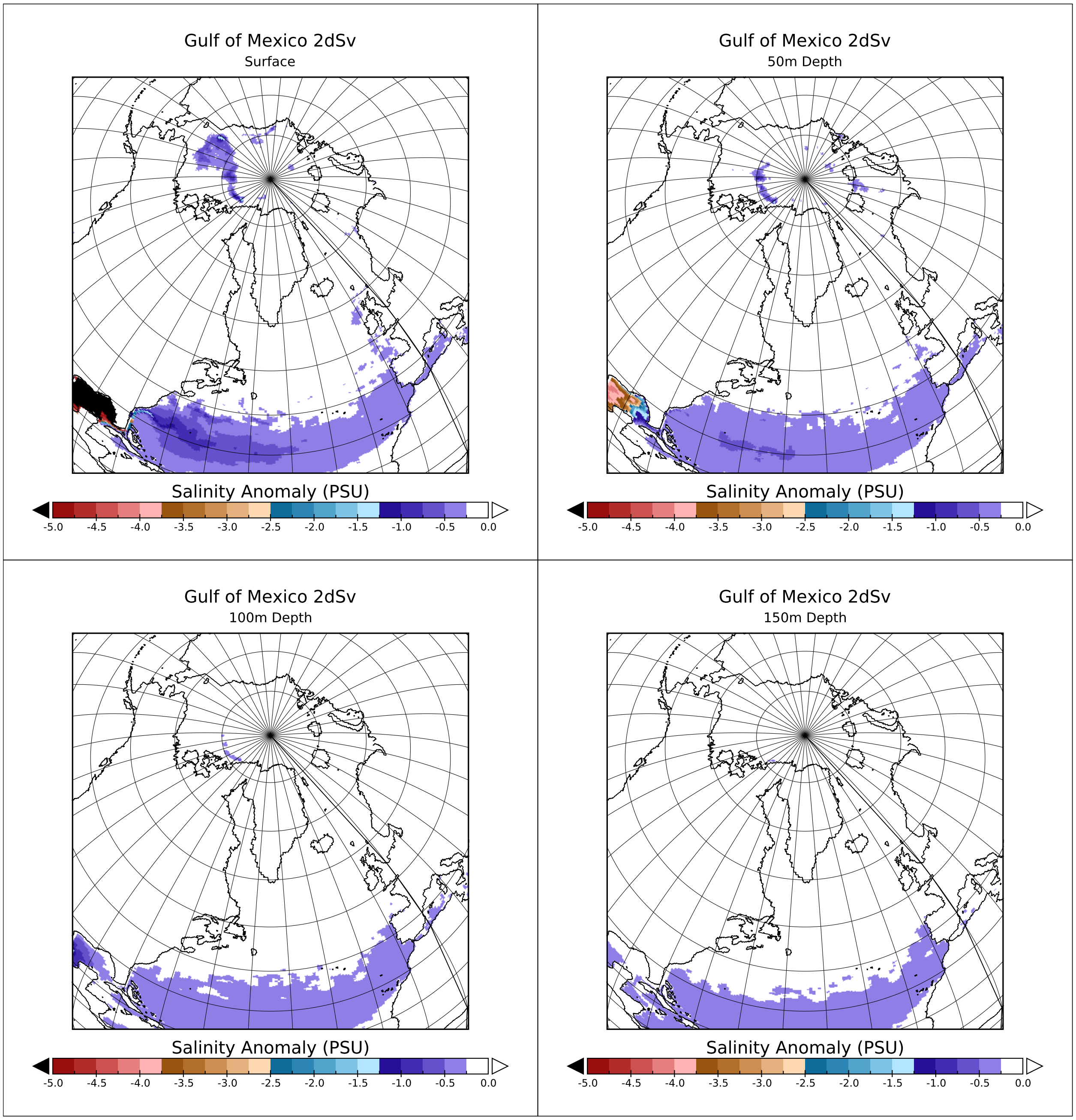

Figure S9: Salinity anomaly distribution at a selection of depths for the Open Bering Strait Gulf of Mexico 2dSv continual injection scenario. This distribution is the average of the anomaly field over the last 5 years of model integration.

S2 Model Drift

For the Barents-Kara sea region we observe a maximum drift of ≈ 0.75psu/a for the open Bering Strait YD case and a maximum of ≈ 0.3psu/a for the closed Bering Strait YD case. The drift is calculated over the duration of the respective control run. This trend is observed in the region directly where the surface runoff is introduced into the model and only in the uppermost ≈ 50m of the water column, with the greatest drift present in the surface layer. For the drift of ≈ 0.75psu/a for the open Bering Strait YD case the magnitude reduces by an order of magnitude at the 30m depth. Elsewhere in the simulation the calculated trend is generally below 0.05psu/a, a trend which may be an artefact of the short run time and reflect ongoing longer timescale internal variability.

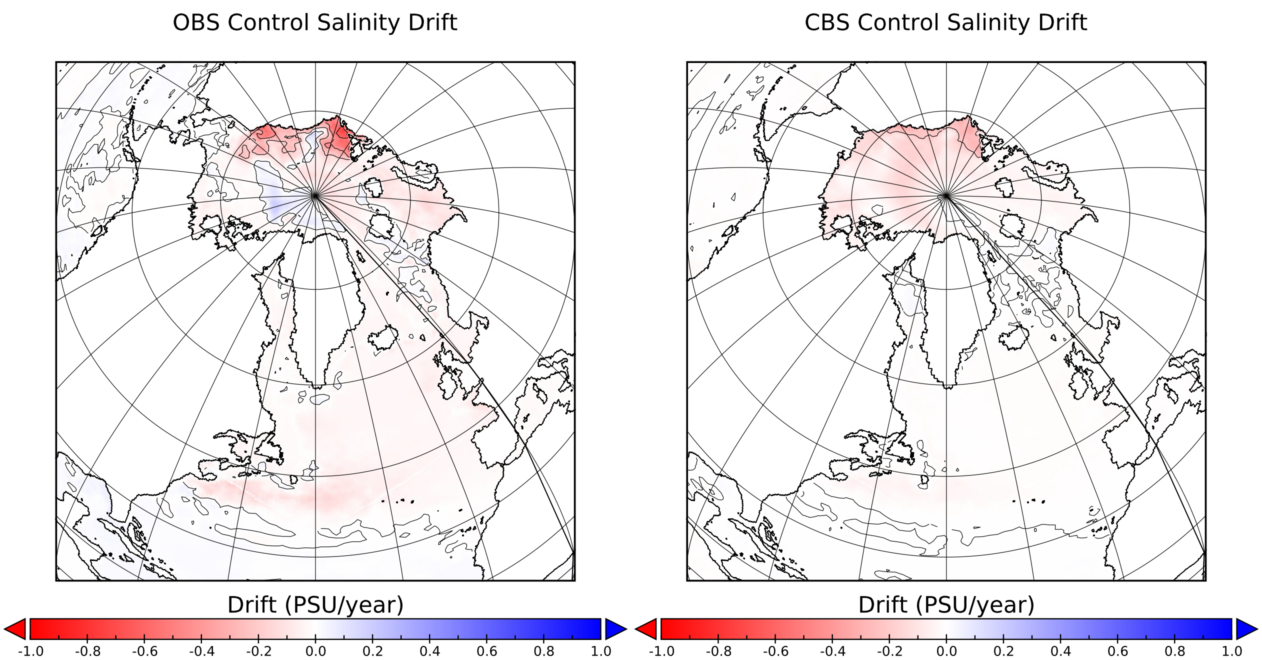

Figure S10: Drift for each of the control runs at the ocean surface calculated over the duration of the control run. Major scale intervals are contoured, most contours denote the 0-line. Continental outlines reflect the land-sea mask as used in each of the control simulations and are identical with the exception of the regions surrounding the Bering Strait. The drift is accounted for as part of the fingerprint processing routine. There is correspondence between the observed drift and the sources of runoff in the model boundary conditions, but is more noticeable in the open Bering Strait configuration.

S3 AMOC Discussion

Since the focus of the study is the surface transport of freshwater, here we discuss the immediate impact of freshwater on rates of DWF and AMOC purely for context. This is done given the significant limitations in using this metric for such short durations, which renders these simulations unsuitable for examination of AMOC and deeper ocean trends. The simulated state of the AMOC is shown in fig. S11. The AMOC in the control simulations shows an overall similar structure (not shown) but weaker values compared to comparable high-resolution members of the multi-model, present-day ensemble in Hirschi et al. [2020]. The strength of the AMOC at 26N in the control simulations is around 4Sv with a one-sigma annual variation of 1Sv, and a strong seasonality. Using 26N to coinicide with previous studies and the RAPID array results in an offset of -6Sv relative to the peak as is common in studies where this feature can be adequately resolved. Consistently with Hu et al. [2015], the CBS control run shows a stronger AMOC than OBS when examined using a 1 year running mean. However, unlike previous studies (e.g. Condron and Winsor [2012]), freshwater forcing in the injection simulations does not influence the AMOC variability or the southward flow from the Labrador Sea above the threshold of internal variability on the time scales examined. The weak AMOC values obtained here indicate that the model is operating in a 'Glacial' mode relative to the previous study by Condron and Winsor [2012], which showed AMOC values around 18Sv under present-day boundary conditions. The ocean operating in a glacial mode is reasonable given the glacial surface forcing and initialization conditions implemented here, although it is unlikely that in reality the ocean was in such a state just prior to the Younger Dryas [McManus et al., 2004]. We expect that otherwise identical simulations performed using surface forcing and initialization conditions more consistent with the start of the Younger Dryas would generate more realistic AMOC values under both control and forcing conditions. Relative to a stronger AMOC we would expect that Gulf Stream, which is highlighted in the main manuscript as being a key feature to reducing meridional transport of freshwater, would be both shifted northwards and closer to shore [Caesar et al., 2018]. However, this does not change the impact of the Gulf Stream on our simulations or conclusions.

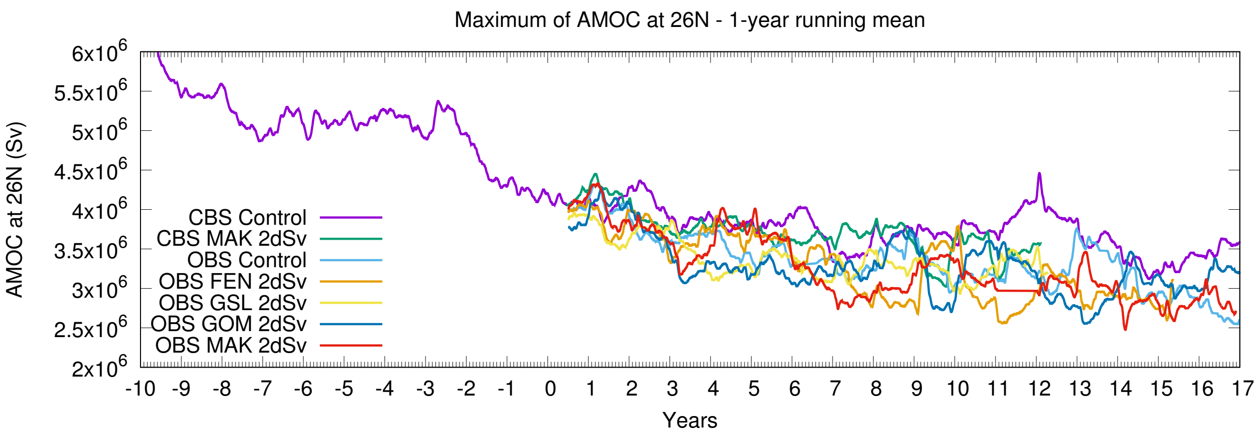

Figure S11: AMOC calculated as the maximum of the meridional overturning stream function at 26N, to coincide with the RAPID array, at depths below 700m. Comparing to the more common metric of maximum of the meridional overturning stream function in the North Atlantic basin below 700m, we find a roughly -6Sv offset, that is the AMOC is roughly 9.5Sv rather than 3.5Sv. Timeseries shown are 1 year running means where year 0 is when glacial runoff is introduced into the model. The standard deviation of this time series, calculated annually, ranges between 1-1.5Sv.

S4 Experimental Design Additional Information

Run name	Bathymetry	Freshwater Forcing	Purpose	Duration (years)	Parent Run
LGMCS510	As in Condron & Hill 2014	None	Spin-up and Preliminary investigations	20	Hill and Condron [2014] Control (not end of simulations)
LGMCS510 YD13kaControl	13kaBP GLAC (CBS)	None	LGM → YD spin up	10	LGMCS510 (T&S field restart due to modified bathymetry)
YDCS510 Control	13kaBP GLAC (CBS)	None	YD CBS Spin-up and control	33	LGMCS510 YD13kaControl
YDCS510 ERA40	13kaBP GLAC (CBS)	None	LGM vs. PD wind comparison	20	LGMCS510 YD13kaControl
YDCS510 ERA40 OBS GOM 0p2C	13kaBP GLAC (CBS)	None	ERA40 Mississippi River Outlet Forcing	10	YDCS510 ERA40 (at year 10)
YDCS510 openBeringControl	13kaBP GLAC (OBS)	None	YD OBS Spin-up and control	33	LGMCS510 YD13kaControl
YDCS510 0p2SvMack	13kaBP GLAC (CBS)	2dSv Mackenzie River (221.25E, 71.15N)	Mackenzie River Outlet Forcing	24	YDCS510 Control (at year 10)
YDCS510 openBering 0p2MackRiver	13kaBP GLAC (OBS)	2dSv Mackenzie River (221.25E, 71.15N)	Mackenzie River Outlet Forcing	23	YDCS510 openBering-Control (at year 10)
YDCS510 OBS FEN 0p2C	13kaBP GLAC (OBS)	2dSv Fennoscandia (2.5E, 63.6N)	Fennoscandian Forcing	22	YDCS510 openBering-Control (at year 10)
YDCS510 OBS GSL 0p2C	13kaBP GLAC (OBS)	2dSv Gulf of St. Lawrence (298.75E, 47.6N)	Gulf of St. Lawrence Outlet Forcing	23	YDCS510 openBering-Control (at year 10)
YDCS510 OBS GOM 0p2C	13kaBP GLAC (OBS)	2dSv Mississippi River (271.25E, 27.8N)	Mississippi River Outlet Forcing	23	YDCS510 openBering-Control (at year 10)

Table S1: A summary of all the runs conducted in this investigation. All runs (excepting YDCS510 ERA40 and YDCS510 ERA40 OBS GOM 0p2C which used ERA40 wind fields) use the same surface forcing as in Hill and Condron [2014] which corresponds with Last Glacial Maximum conditions. Data from 'LGMCS510' and 'LGMCS510 YD13kaControl' are not shown in any figures.

S5 Effects of modern wind forcing on the Gulf Stream

To explore the impact that our overly zonal Gulf Stream has on one of the injection locations most sensitive to this feature we performed a pair of brief sensitivity runs. These sensitivity use an identical configuration to our other YDCS510 runs except the wind forcing has been replaced by fields from the ERA40 atmospheric re-analysis [Kållberg et al., 2004]. We observe that the salinity anomaly field is zonal as in our other simulations but with additional freshwater being transported north-east in the direction of the more modern path of the Gulf Stream. Examining the sea surface velocity fields between the ERA40 Control and the YD Open Bering Strait Control we find that the YD OBS Control has faster surface currents relative to the ERA40 simulation, as well as a Gulf Stream located $\approx 5°$ closer to the equator. Despite these differences, the blocking behaviour observed in the YDCS510 OBS GOM run and discussed in the main text remains.

S6 Hosing difference approximation

When comparing the freshening effect of direct injection into the regions of interest, we use the following: we assume that the freshwater displaces existing seawater from the regions, that the injection region is evenly inundated with freshwater, and the freshwater is evenly mixed over the top 50m of the water column. Also, given this is a very simplified approximation, we assume the density of sea water and freshwater are the same, neglecting the $O(3\%)$ error.

$$S_{displaced} = q_{fw} \Delta t S_{avg} \rho_w \tag{1}$$

$$S_{total} = A \Delta z \rho_w \tag{2}$$

$$S_{diff} = (S_{total} - S_{displaced})/(A \Delta z \rho_w) \tag{3}$$

Where $S_{displaced}$ is the salt we are displacing with freshwater, S_{total} is the total salt in the volume, S_{diff} is the resulting salinity difference, S_{avg} is the average salinity of the region (taked directly from the model and over the top 50m), q_{fw} is the freshwater flux (2dSv in our calculations), Δt is the time over which the flux is considered (1 year), ρ_w is the density of water we use 1000kg/m^3, A is the area of the region, and Δz is the depth which we are considering the freshwater is mixing (50m).

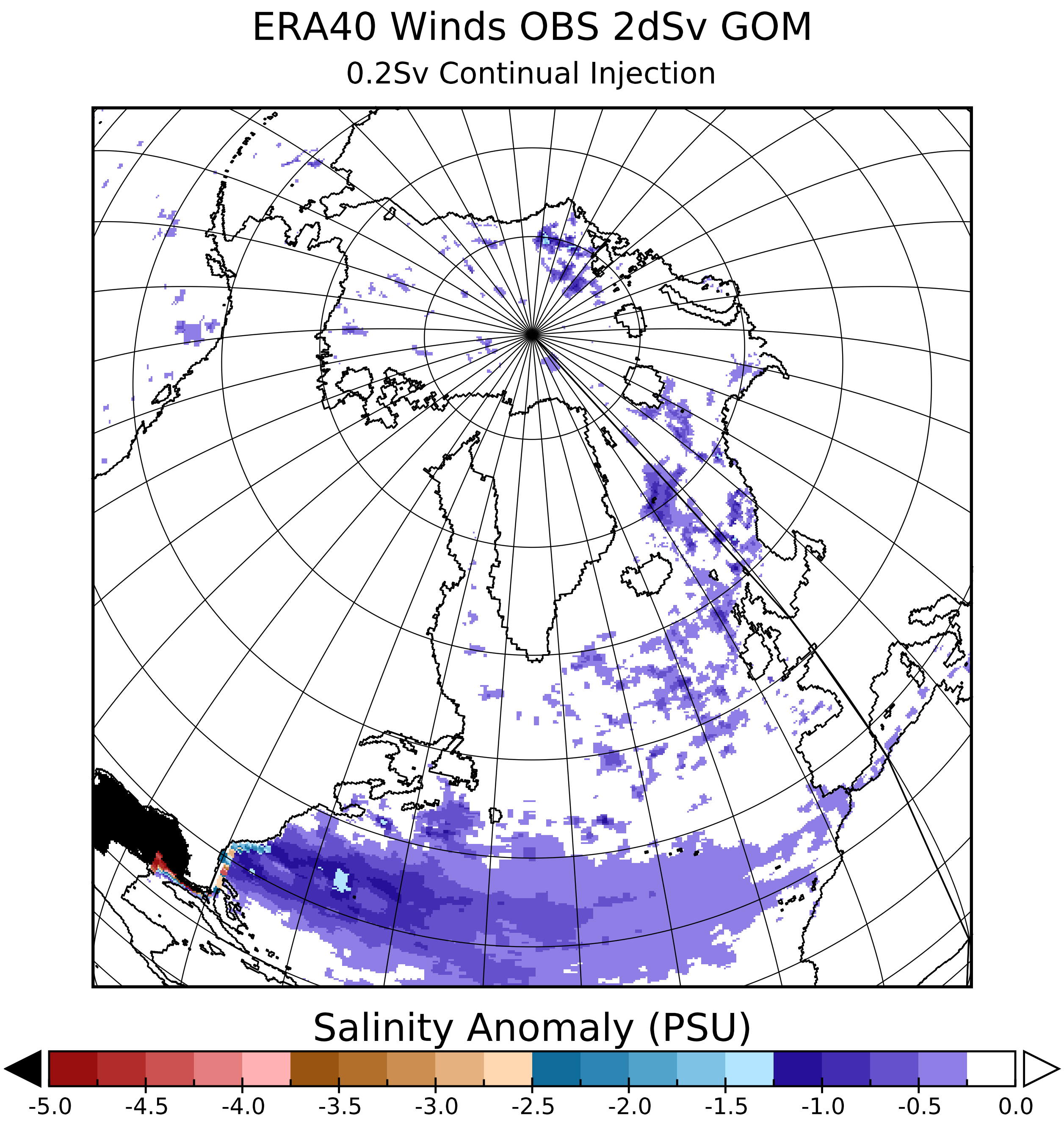

Figure S12: Sea surface salinity anomaly distribution for our OBS 2dSv GOM injection run with ERA40 surface wind forcing. This distribution is the average of the anomaly field over the last year of model integration.

References

L. Caesar, S. Rahmstorf, A. Robinson, G. Feulner, and V. Saba. Observed fingerprint of a weakening atlantic ocean overturning circulation. *Nature*, 556(7700):191196, Apr 2018. ISSN 1476-4687. doi: 10.1038/s41586-018-0006-5. URL `http://dx.doi.org/10.1038/s41586-018-0006-5`.

A. Condron and P. Winsor. Meltwater routing and the younger dryas. *Proceedings of the National Academy of Sciences*, 109(49):1992819933, Nov 2012. ISSN 1091-6490. doi: 10.1073/pnas.1207381109. URL `http://dx.doi.org/10.1073/pnas.1207381109`.

Jenna C. Hill and Alan Condron. Subtropical iceberg scours and meltwater routing in the deglacial western north atlantic. *Nature Geoscience*, 7(11):806810, Oct 2014. ISSN 1752-0908. doi: 10.1038/ngeo2267. URL `http://dx.doi.org/10.1038/ngeo2267`.

Jol J.M. Hirschi, Bernard Barnier, Claus Bning, Arne Biastoch, Adam T. Blaker, Andrew Coward, Sergey Danilov, Sybren Drijfhout, Klaus Getzlaff, Stephen M. Griffies, and et al. The atlantic meridional overturning circulation in high-resolution models. *Journal of Geophysical Research: Oceans*, 125(4), Apr 2020. ISSN 2169-9291. doi: 10.1029/2019jc015522. URL `http://dx.doi.org/10.1029/2019JC015522`.

Aixue Hu, Gerald A. Meehl, Weiqing Han, Bette Otto-Bliestner, Ayako Abe-Ouchi, and Nan Rosenbloom. Effects of the bering strait closure on amoc and global climate under different background climates. *Progress in Oceanography*, 132:174196, Mar 2015. ISSN 0079-6611. doi: 10.1016/j.pocean.2014.02.004. URL `http://dx.doi.org/10.1016/j.pocean.2014.02.004`.

Per Kållberg, Adrian Simmons, Sakari Uppala, and Manuel Fuentes. The era-40 archive. *ERA-40 project report series*, 17:31, 2004.

J. F. McManus, R. Francois, J.-M. Gherardi, L. D. Keigwin, and S. Brown-Leger. Collapse and rapid resumption of atlantic meridional circulation linked to deglacial climate changes. *Nature*, 428(6985):834837, Apr 2004. ISSN 1476-4687. doi: 10.1038/nature02494. URL `http://dx.doi.org/10.1038/nature02494`.